Nanoscale

Accepted Manuscript

This article can be cited before page numbers have been issued, to do this please use: R. Morales, S. T. Bromley, I. Demiroglu and F. Viñes, *Nanoscale*, 2025, DOI: 10.1039/D4NR05206D.

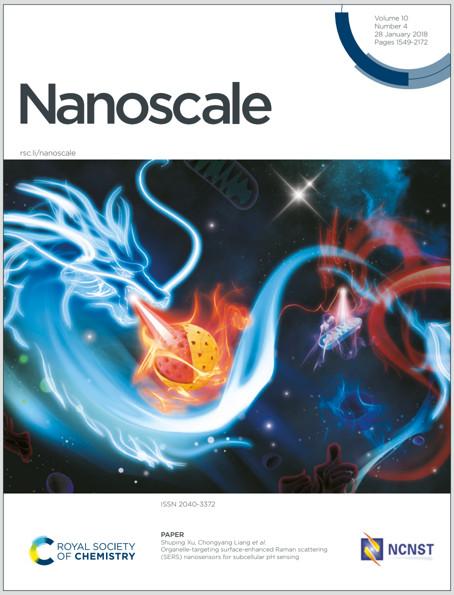

ROYAL SOCIETY
OF CHEMISTRY

rsc.li/nanoscale

View Article Online
DOI: 10.1039/D4NR05206D

Tuning the Electronic Properties of ZnO Nanofilms via Strain-induced Structural Phase Transformations and Quantum Confinement

Raul Morales-Salvador[1], Ilker Demiroglu[2], Francesc Viñes[1], Stefan T. Bromley*[1,3]

[1]*Departament de Ciència de Materials i Química Física & Institut de Química Teòrica i Computacional (IQTC), Universitat de Barcelona, c/ Martí i Franquès 1-11, 08028 Barcelona, Spain.*

[2] *Department of Advanced Technologies, Eskisehir Technical University, 2 Eylül kampüsü, 26555 Eskişehir, Turkey*

[3] *Institució Catalana de Recerca i Estudis Avançats (ICREA), Passeig de Lluís Companys, 23, 08010 Barcelona (Spain).*

*Corresponding author: s.bromley@ub.edu

Abstract

ZnO nanostructures have huge potential in a wide range of technologies, including photocatalysis, optoelectronics, and energy harvesting. ZnO commonly exhibits the wurtzite polymorphic phase (wz-ZnO), and one of the few inorganic materials where nanoscale structural phase engineering has revealed alternative polymorphs. These structurally novel nanophases also have properties (e.g. mechanical, electronic) that differ from those of wz-ZnO, and thus may pave the way to new applications. Here we follow the strain-induced transformation between the body centred cubic phase (BCT-ZnO) and the graphitic phase (g-ZnO), which has been experimentally demonstrated in ZnO nanowires. Using free-standing ZnO nanofilms a reference nanosystem, we use density functional theory based calculations to follow the BCT-ZnO ↔ g-ZnO phase transformation relative to systematic changes in in-plane biaxial strain and nanofilm thickness. Tensile strain favours the BCT-ZnO phase, whereas compressive strain induces the transformation to the g-ZnO phase. As the application of nanoscale ZnO usually take advantage of its semiconducting nature, we mainly focus on the variance of the band gap and the character

View Article Online
DOI: 10.1039/D4NR05206D

the band edges. Our work strongly features the use of Crystal Orbital Hamilton Population (COHP) analysis, which helps provide a uniquely detailed understanding of this complex nanosystem based on orbital overlap. We use this approach to reveal how strain and quantum confinement (through nanofilm thickness) have distinct and significant effects the on the structural and electronic properties of both BCT-ZnO and g-ZnO phases. The latter phase is particularly interesting as it involves a subtle competition between two structural phases (the layered-ZnO and hex-ZnO phases). These phases can be distinguished by their respective orbital overlap characteristics which, in turn, can be finely tuned by strain and thickness. We propose that the rich electronic properties of this nanosystem can be interpreted through a monolayer superlattice model in which localised surface states and more spatially delocalised quantum confined states compete. More generally our work illustrates how the intricate interplay of strain, quantum confinement and structural phase transformations in an inorganic nanosystem can be analysed and understood through use of COHP analysis of orbital overlap contributions.

View Article Online
DOI: 10.1039/D4NR05206D

Introduction

Nanoscale materials often exhibit different crystalline atomic orderings (*i.e.* polymorphs) to those observed in the respective macroscopic solids.[1] The structures and properties of low dimensional nanomaterials (*e.g.* nanofilms, nanowires) can also be tuned by mechanical strain.[2] Combining size and strain thus provides a flexible approach for structural phase engineering of nanomaterials in which emergent properties (*e.g.* mechanical, electronic) can lead to new applications.[3] Here, we focus on zinc oxide (ZnO) which is highly amenable to nanostructuring[4] and has huge potential in a wide range nanoscale applications (*e.g.* photocatalysis, optoelectronics, energy harvesting).[5] ZnO is also one of the very few inorganic materials for which nanoscale phase engineering has been experimentally demonstrated using both size[6] and strain.[7] ZnO has thus become an archetypal system for theoretically predicting the viability of new stable polymorphic phases by system size reduction[8,9,10,11,12,13,14] and/or by nanostructuring.[15,16,17,18]

The possibility of novel nano-stabilised structural phases in ZnO started with the theoretical prediction of a so-called graphitic polymorph (g-ZnO) in unsupported nanofilms,[8] which was subsequently confirmed in experiments on metal-supported ZnO nanofilms.[6] The g-ZnO phase consists of *a*-*b* planar $(ZnO)_3$-based hexagonally ordered layers stacked in the *c* direction. We note that unlike graphite, which has a staggered AB stacking of hexagonal layers, g-ZnO exhibits an eclipsed AA stacking. For free-standing nanofilms, g-ZnO is predicted to be the most energetically stable ZnO polymorph for stacks of up to three planar hexagonal layers (*i.e.* $N \leq 3$ layers). g-ZnO nanofilms have attracted interest with respect to possible chemical applications (*e.g.* strain-thickness reactivity control,[19,20] CO_2 photoreduction[21]). However, such studies rarely consider the possibility of transformations to other competing polymorphic phases.

For nanofilms with $N \geq 4$, it becomes more energetically favourable for the layers in the g-ZnO phase to slightly buckle and bond with one other. The different possible nanofilm polymorphs available at this structural phase transformation can enumerated by systematically varying the bonding patterns between stacked hexagonal layers while maintaining the AA stacking of g-ZnO.[9] For four layers, the lowest energy polymorphs resulting from this search are found to be a class of polytypes based on the body centred cubic phase (BCT-ZnO).[9] This finding is in line with other studies where the transformation from g-ZnO to BCT-ZnO in nanofilms with $N = 4 - 16$ has been calculated to be effectively barrierless at finite temperatures.[13,11]

The BCT-ZnO phase is also predicted to be more stable than pristine wz-ZnO in *c*-oriented freestanding nanofilms with $N \leq 27$.[11] The relatively low stability of *c*-oriented wz-ZnO nanofilms in this thickness range is due to the energetically costly electronic imbalance induced by the

View Article Online
DOI: 10.1039/D4NR05206D

terminating (0001) and $(000\bar{1})$ polar surfaces.[13,22] Calculations of nanofilms possessing pristine as-cut polar surfaces will attempt to compensate this imbalance by internal charge transfer from one polar surface to another leading to spurious surface metallisation.[13] This is a relatively inefficient stabilization mechanism and clean (*i.e.* ligand-free) ZnO polar surfaces are instead experimentally observed to structurally reconstruct to achieve stabilization.[23,24] Increasing the stability of polar wz-ZnO nanofilms by surface reconstruction lowers the thickness at which the stability crossover to BCT-ZnO occurs to between 14-16 layers.[9] For *c*-oriented wz-ZnO nanofilms that are thinner than this threshold, it is more effective to stabilize the system via a phase transformation of the whole nanofilm to a non-polar structure. For the thinnest nanofilms this transformation is found to be spontaneous, with pristine wz-ZnO nanofilms with directly relaxing to the g-ZnO structure for $N \leq 4$ and to BCT-ZnO for $N = 5\text{-}6$ layers.[11] Thicker wz-ZnO nanofilms layers with approximately $N = 7\text{-}16$ are metastable in 0 K calculations, but are likely to be thermally or mechanically susceptible to phase transformations to more stable non-polar phases such as BCT-ZnO. In principle, there are some non-polar nanofilm structures that are theoretically predicted to be slightly energetically more stable than BCT-ZnO at 0 K, for the thickness range $N = 7–16$. However, the transformations to such structures from BCT-ZnO have relatively high associated barriers.[13] As such, the relatively easier transitions between g-ZnO/wz-ZnO and BCT-ZnO are likely to dominate in ZnO nanomaterials for moderate temperatures and/or mechanically induced phase transformations.

The favoured wz-ZnO phase in macroscopic systems has a relatively high density. Thus, accessing lower density polymorphs, such as g-ZnO and BCT-ZnO, from wz-ZnO by mechanical means implies the need of significant negative pressures (*i.e.* tensile strain).[25,27] The inherent favorability of BCT-ZnO and g-ZnO in nanosized systems and the easier application of uniaxial/biaxial tensile stress in low dimensional nanostructures (*e.g.* 1D nanowires, 2D nanofilms) thus open opportunities for stress-induced phase control. We also note that with decreasing size, nanomaterials also tend to have fewer structural defect and are thus less susceptible to structural failure under stress.[28] Experimentally, uniaxially stressed wz-ZnO nanowires, are indeed found to display a reversible phase transformations between BCT-ZnO and g-ZnO (hex-ZnO), where the BCT-ZnO phase is predicted to become dominant.[7] Computational modelling studies have also studied similar phase transformations to BCT-ZnO in nanowire systems, induced by either uniaxial strain[29] or bending.[30] Reversible phase transformations between wz-ZnO and BCT-ZnO phases have also been experimentally observed in the outer few layers of non-polar surfaces of wz-ZnO nano-islands.[31]

Considering the technological potential of nano-ZnO and the experimentally confirmed nanoscale stabilisation and structural interconversion of g-ZnO and BCT-ZnO polymorphs, it is

DOI: 10.1039/D4NR05206D

important to understand the properties of this phase-reversible nanosystem. Here, we provide a systematic study of how the g-ZnO ↔ BCT-ZnO phase transformation can be engineered by both biaxial strain and thickness in ZnO nanofilms. We specifically focus on how the electronic structure varies during these size/strain-induced structural changes. By carefully analysing the respective roles of orbital overlap and quantum confinement, we show that this phase-tunable semiconductor nanofilm system allows for highly controllable band gaps and band edges which could open the door to new applications.

Models and Computational Details

We consider isolated periodic slab models to represent free-standing nanofilms of both g-ZnO and BCT-ZnO. This choice avoids the fact that the differing basal plane symmetries of g-ZnO and BCT-ZnO tends to inhibit their phase interconversion when epitaxially supported.[32,33] *N*-layer (hereon abbreviated to *N*L) slab models with $N =$ 3-6, 8, 10, 12, 14, 16 were considered. For both polymorphs *p*(2×2) supercells were used, where each layer is composed of four Zn and four O atoms. To avoid spurious inter-slab interactions, models were isolated in the direction normal to the slab surface by a periodic vacuum spacing of 10 Å.

For few-layer g-ZnO, the interaction between aligned hexagonal layers is non-bonded, as in graphite. However, a very similar phase has been reported with bonded interactions between layers.[9] Although these two forms of g-ZnO are often conflated in the literature, herein we highlight their distinct properties and how they can be revealed and controlled during phase transformations. When required, we distinguish the g-ZnO form with non-bonded layers as the layered phase (layered-ZnO) and the more strongly bound version as the hexagonal phase (hex-ZnO). The models of all considered phases are shown in figure 1.

To calculate the optimized structures and properties of the three phases, periodic density functional theory (DFT) based calculations were carried out using the Perdew-Burke-Ernzerhof (PBE)[34] functional by means of the VASP code.[35,36] We note that the PBE functional has been previously shown to be reliable for evaluating pressure-induced phase transitions between ZnO polymorphs.[37-39] The underestimation of electronic band gaps when using the PBE functional is approximately corrected using a fitted relation between band gap values as calculated using PBE and an accurate many body GW method for a range of ZnO polymorphs.[18] The projector augmented wave approach[40] was used to the describe the core electron density, with all *d* electrons included for Zn atoms. The valence electron density was expanded in a plane wave basis set with a cut-off energy of 500 eV. The Brillouin zone integration was sampled using a 3×3×1 Monkhorst-Pack **k**-grid.[41] The threshold for the electronic convergence criterion was set

View Article Online
DOI: 10.1039/D4NR05206D

to 10^{-4} eV, and geometry optimizations were considered converged when forces acting on atoms were below 0.01 eV Å^{-1}. For calculating band structures, single point calculations of optimised nanofilm structures were employed using a 9×9×1 Monkhorst-Pack **k**-grid. Convergence tests for the chosen calculation parameters can be found in the Electronic Supplementary Information (ESI).

For each slab the in-plane cell parameters were constrained at range of fixed values to model a range of in-plane biaxial strains between -10% (*i.e.* compression) and +10% (*i.e.* tension). For each strain the coordinates of all atoms and the out-of-plane *c*-parameter of the supercell were allowed to fully relax without symmetry constraints.

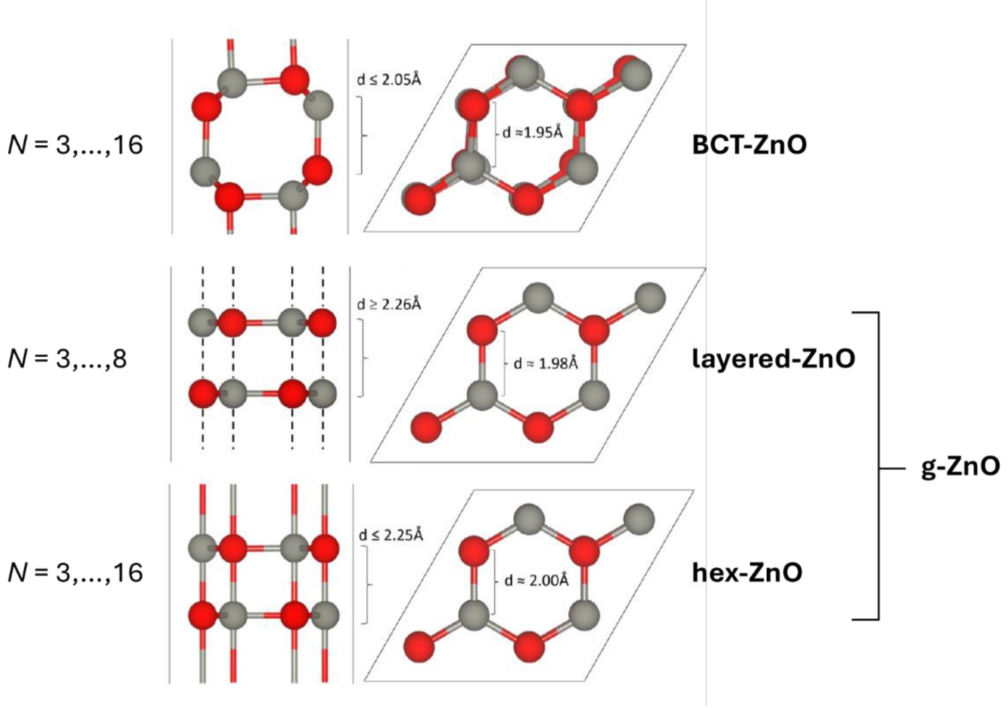

Figure 1. Atomic positions for 2 layers of the: BCT-ZnO (upper) and the layered- and hex- forms of g-ZnO (lower). Grey lines indicate the boundary of the periodic simulation cell (left: in-plane view, right: c-axis view) The listed numbers of layers (N) for each case indicates the thickness range for which the respective structure could be stabilised for some range of in-plane strain. Atom colour key: Zn – grey, O – red.

To analyse the bonding in the studied polymorphs, we employed COHP (Crystal Orbital Hamilton Population) analysis[42,43] as implemented in the LOBSTER code.[44] This methodology partitions the energy of electronic bands into contributions from overlapping orbitals. Specifically, for orbitals centred on neighbouring atoms, COHP provides a quantitative measure of energy-lowering bonding (negative) contributions and energy-raising antibonding (positive) contributions. Note that energetically neutral non-bonding makes a zero COHP contribution.

View Article Online
DOI: 10.1039/D4NR05206D

Consequently, energy-resolved COHP analyses provide a way to interpret band structures in terms of local chemical interactions.

For a more detailed analysis of chemical bonding, the COHP approach can be directionally resolved whereby the energy of a given band is decomposed into individual contributions from each **k**-point. The resulting kCOHP analysis mathematically distinguishes between on-site and off-site contributions in the following way:

$$E_{i\mathbf{k}} = \sum_{n} \mathrm{COHP}^{i\mathbf{k}} \quad (1),$$

$$E_{i\mathbf{k}} = \mathrm{COHP}^{i\mathbf{k}}_{on-site} + \mathrm{COHP}^{i\mathbf{k}}_{off-site} \quad (2),$$

$$\mathrm{COHP}^{i\mathbf{k}}_{on-site} = \sum_{n_i,n_i} \mathrm{COHP}^{i\mathbf{k}} \quad (3),$$

$$\mathrm{COHP}^{i\mathbf{k}}_{off-site} = \sum_{n_i,\, n_j} \mathrm{COHP}^{i\mathbf{k}} \quad (4),$$

where $\mathrm{COHP}^{i\mathbf{k}}$ are the individual **k**-dependent COHP contributions. The on-site term corresponds to intra-atomic interactions, such as the classical electron-electron and electron-ion interaction. The off-site term originates from the interatomic interactions between pairs of atoms in a given solid-state structure. The off-site term is assigned to be negative when the interaction between atoms is bonding and tends to stabilize the corresponding band. Conversely, a positive value corresponds to band-destabilising antibonding interactions. When considering mechanical strain, we expect that decreasing the distance between bonded atoms will decrease (increase) the energy of the corresponding band for bonding (antibonding) interactions, and *vice versa*. Since non-bonding states have an overlap integral of zero, they are invariable under strain.[45]

Results and Discussion

Using the above-described slab models we systematically vary the nanofilm thickness and in-plane strain. For all considered thicknesses, a polymorphic g-ZnO ↔ BCT-ZnO phase transformation is also observed within the range of in-plane strain considered. Below, we follow how these three interacting factors lead to complex changes in energetic stability, structure, electronic properties and reactivity.

Structure and energetics

In Figure 2 we plot the calculated relative energy of the in-plane strained ZnO nanofilms of varying thickness with respect to the energy of bulk BCT-ZnO. For each thickness we define zero strain at the point of minimum energy on each relative energy curve which, all cases,

View Article Online
DOI: 10.1039/D4NR05206D

corresponds to the fully relaxed BCT-ZnO phase. With increasing nanofilm thickness, the curves progressively shift to lower energies indicating an expected stabilisation towards the corresponding bulk phase. For in-plane compression until -8% the BCT-ZnO phase remains structurally stable for all nanofilm thicknesses. Upon in-plane biaxial tension the BCT-ZnO phase is susceptible to a phase transformation to the g-ZnO phase. We note that there is no obvious sign of a differentiation between the layered- and hex- forms of the g-ZnO phase in the relative energy curves. For the thinnest 3L BCT-ZnO slab, we find that the transformation to g-ZnO can be achieved with +1.3% strain. However, with increasing thickness the strain required to induce the transformation increases to approximately +5.5% for the thickest 16L nanofilm. This change is in-line with the increasing energy difference between the BCT-ZnO and g-ZnO phases with increasing thickness. Apart from the thinnest 3L nanofilm, the strain-induced BCT-ZnO → g-ZnO transformation for thicker nanofilms leads to an increasingly positively strained g-ZnO phase with respect to its minimum energy on an extrapolated energy versus strain curve. This implies that it would be difficult to stabilise fully relaxed g-ZnO nanofilms due to their mechanical instability to transform into the BCT-phase. We note that systematic computational exploration of biaxially strained nanofilms can be used to search for such instabilities and thus find new polymorphic phases in a simulated mechanical annealing approach.[46]

For better understanding how to physically induce the BCT-ZnO and g-ZnO phase transformation by applied tensile stress, we have calculated the in-plane biaxial modulus for the 5L nanofilm to be 138.5 GPa. This would imply that a tensile stress of 1.4 GPa would be needed for each +1% of biaxial strain of the 5L BCT-ZnO nanofilm. This is comparable to the 5 - 15 GPa of uniaxial tensile stress used in experiments on ZnO nanowires to induce BCT-ZnO phase transformations with corresponding strains of approximately 2-5%.[7]

View Article Online
DOI: 10.1039/D4NR05206D

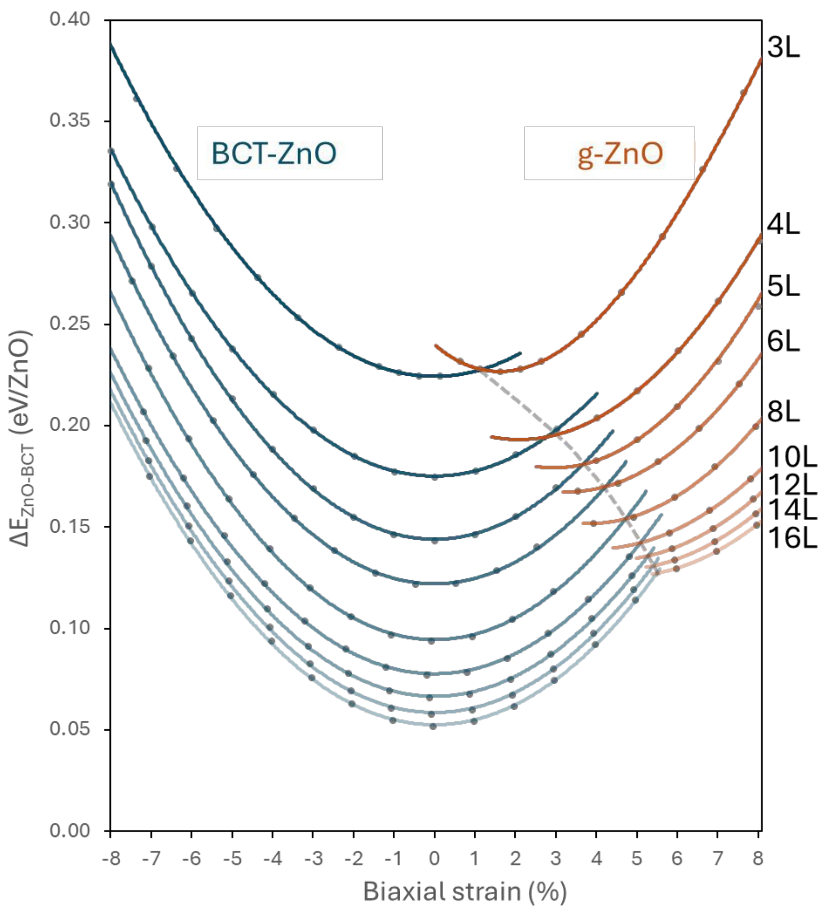

Figure 2. Relative energy (relative to bulk BCT-ZnO per ZnO unit) of nanofilms with respect to varying both in-plane biaxial strain and nanofilm thickness. Solid lines are guides to the eye and follow the calculated black datapoints. Blue lines follow datapoints corresponding to the BCT-ZnO phase and orange lines follow datapoints corresponding to the g-ZnO phase. The dashed grey line follows the strain/thickness conditions at the BCT-ZnO ↔ g-ZnO energetic stability transition.

In Figure 3 we follow how the *c*/*a* lattice parameter ratio varies with respect to in-plane strain for selected representative nanofilm thicknesses of N = 5, 8, 12, 16. For the data corresponding to the BCT-ZnO phase, the nanofilms show a monotonic linear decrease of their *c*/*a* ratio from an in-plane compression of -8% up until the tensile strain corresponding to the transformation to the g-ZnO phase. At this point the *c*/*a* ratio abruptly decreases and then continues to decrease linearly with a slightly shallower slope. Increasing the nanofilm thickness results in a progressively steeper slopes of the linear trends in the *c*/*a* ratio for both phases. For materials with a positive Poisson ratio, increasing the *a* and *b* parameters via in-plane tensile strain will cause a corresponding reduction in the *c*-parameter, and vice versa. We note that, as for the energetic stability (see Fig. 2), the strain/thickness-dependent tendencies of the *c*/*a* ratio in the region of g-ZnO stability show no obvious signs of distinct hex-ZnO and layered-ZnO forms.

View Article Online
DOI: 10.1039/D4NR05206D

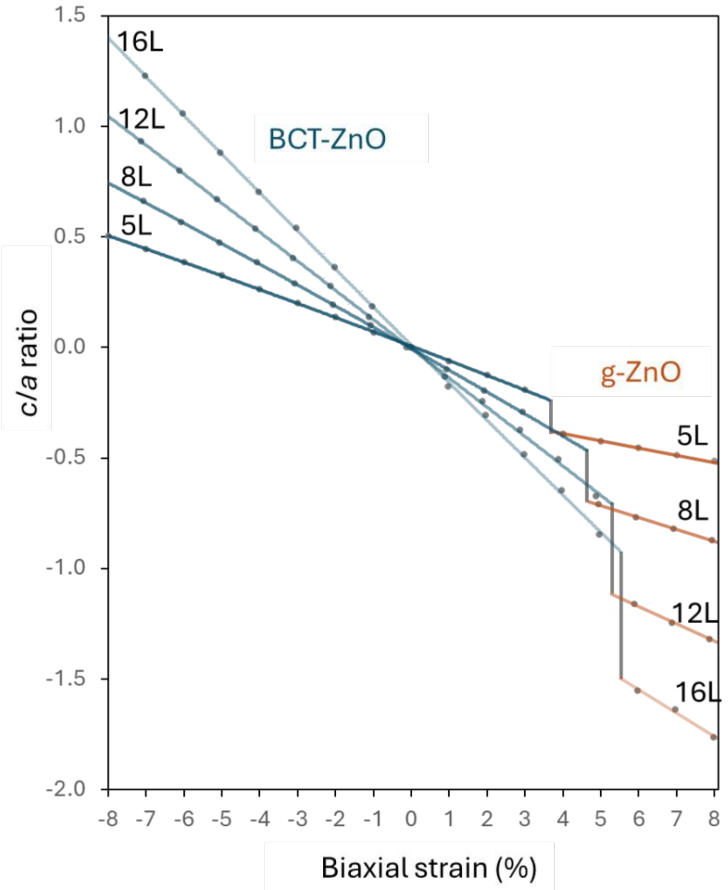

Figure 3. Dependence of *c*/*a* ratio on in-plane strain for four selected nanofilm thicknesses. Solid lines are guides to the eye and follow the calculated black datapoints. Blue lines follow datapoints corresponding to the BCT-ZnO phase and orange lines follow datapoints corresponding to the g-ZnO phase.

From an atomistic perspective, in-plane compression of the unstrained BCT-ZnO phase tends to increase the buckling of the *a*-*b* layers while maintaining the bonding connectivity of the BCT phase. However, in-plane tensile strain leads to more complex bonding changes. In Figure 4 we examine the strain-induced structural response of the g-ZnO phase from a chemical bonding perspective for the thinnest 3L system. Increasing tensile strain on the unstrained BCT-ZnO phase will first tend to flatten the *a*-*b* layers favours the transition to the layered-ZnO. For the 3L system this occurs at +1% strain where the average interlayer spacing has its maximum of 2.43 Å. At this point a COHP analysis of the Zn4s-O2s bonding (see insets to Figure 4) shows that the in-plane bonding contribution is larger than the out-of-plane bonding contribution. Although increasing the in-plane strain increases the in-plane Zn-O bond distances and quickly brings the layers closer together, the dominance of in-plane bonding over out-of-plane bonding persists until a strain of +6%. Here, the interlayer spacing is reduced by 0.2 Å to 2.25 Å, at which the out-of-plane bonding COHP contribution becomes equal to the respective in-plane

View Article Online
DOI: 10.1039/D4NR05206D

contribution. Further increase in strain results in a more gradual linear decrease in the interlayer spacing where the out-of-plane bonding COHP contribution dominates indicating transition to the hex-ZnO phase with interlayer Zn-O bonds. A similarly large difference in interlayer spacing between relaxed 6L layered-ZnO films (2.37 Å) and the bulk hex-ZnO phase (2.25 Å) was reported in ref. 47 (where both phases are referred to as the h-BN phase), where it is noted that this structural response is inverse to that found in non-layered ZnO nanofilms. This behaviour also suggests that out-of-plane uniaxial compression in the *c*-direction would also be a possible means to control the BCT-ZnO ↔ layered-ZnO/hex-ZnO phase transformation in this system. Indeed, several DFT studies have examined how uniaxial compression in the c-direction can induce phase wz-ZnO → g-ZnO transformations in the bulk[48] and in nanowires.[9,49] For progressively thicker nanofilms, the strain-induced BCT-ZnO → g-ZnO transformation occurs when the g-ZnO phase is increasingly positively strained away from its most relaxed structure. As such, the range of strain for which the layered-ZnO phase can be stabilised by tensile strain rapidly reduces with nanofilm thickness.

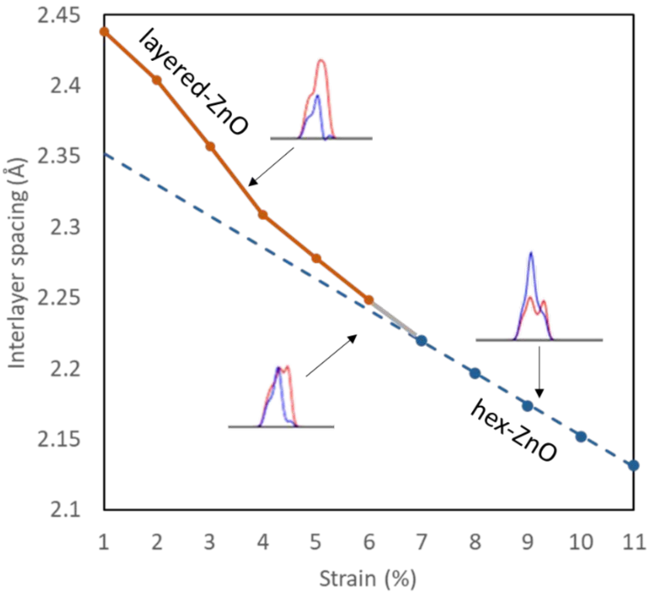

Figure 4. Dependence of average interlayer spacing on in-plane strain for the 3L system. The inset plots show the characteristic in-plane (red) and out-of-plane (blue) bonding COHP contributions for different strain regimes.

Electronic structure

In-plane biaxial strain

View Article Online
DOI: 10.1039/D4NR05206D

In Figure 5 we show how the minimum energy gap (E_{gap}) between the valence band maximum (VBM) and the conduction band minimum (CBM) varies throughout a biaxial strain range of -8% to +10% for all considered nanofilms. As noted above, the reported E_{gap} values have been corrected using a fitted linear relation between (underestimated) PBE-calculated gap values and more accurate gap values calculated using many-body GW calculations.[18] Three different regions can be clearly distinguished, each corresponding to a distinct ZnO phase. Starting from the most in-plane compressed BCT-ZnO nanofilms at –8% biaxial strain, the E_{gap} values range from 2.64 eV for the thickest 16L nanofilm to 3.18 eV for the thinnest 3L nanofilm. Increasing the in-plane lattice parameters leads to a near linear increase in the E_{gap} values up until the phase transformation to the layered-ZnO. Just before this transition, the E_{gap} values for the BCT-ZnO nanofilms range from 3.26 eV (16L) to 4.01 eV (3L). Throughout their respective stable strain regimes, all the BCT-ZnO nanofilms are found to possess a direct E_{gap} at the **Γ** point in reciprocal space.

Upon the strain-induced phase transformation to the layered-ZnO phase the E_{gap} values for each nanofilm sharply increase. This increase ranges from approximately +0.4 eV for the thickest films to approximately +0.15 eV for the 3L nanofilm. Like the BCT-ZnO phase the layered-ZnO phase has a direct band gap at the gamma point in reciprocal space. In the range of strains for which different nanofilms exhibit a stable layered-ZnO phase, the E_{gap} values are relatively stable, with only small gap decreases with increasing positive strain. Further positive strain leads to a transformation of all nanofilms to the hex-ZnO phase. It is found that the layered-ZnO → hex-ZnO phase transformation is also linked to an electronic transition from a direct to indirect band gap. The transformation to the hex-ZnO phase also marks a significant increase in the rate of E_{gap} magnitude reduction with increasing in-plane tension.

View Article Online
DOI: 10.1039/D4NR05206D

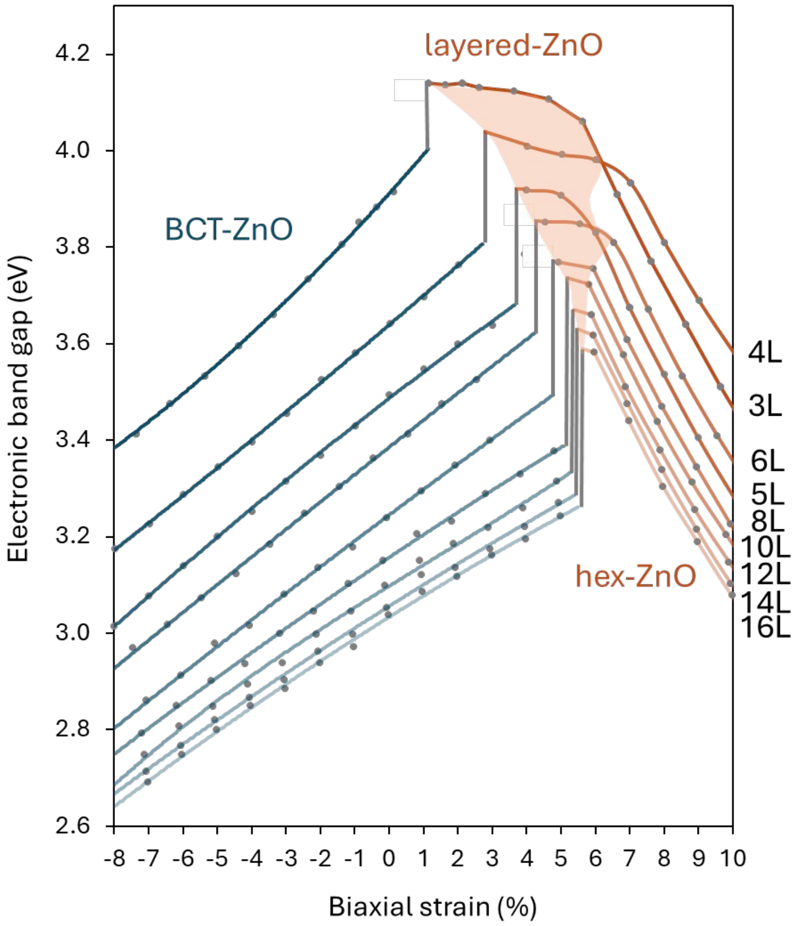

Figure 5. Variation of E_{gap} versus biaxial strain. The PBE-calculated E_{gap} values have been corrected following the approach in ref. 18. The orange shaded area indicates the approximate region of stability of the layered-ZnO phase.

The transition from a direct (layered-ZnO) to an indirect gap (hex-ZnO) can be understood due to the strain-dependent competition between in-plane and out-of-plane Zn-O antibonding bands in the two respective materials (see above). Each of these bands give rise to two distinct O2p contributions to the VBM at **k**-points **Γ** and **T**. Competition between in-plane and out-of-plane antibonding causes corresponding changes in the VBM and a shift between a direct gap (layered-ZnO) and an indirect band gap (hex-ZnO). In Figure 6**,** we show this situation with bands calculated for the 5L nanofilm case. Here, the red band has its main contribution at **Γ** from antibonding orbital overlap from in-plane Zn-O bonds. Conversely, at **T**, antibonding overlap from out-of-plane Zn-O bonds are the major contributor to the green band. With an increase of tensile biaxial strain, the in-plane Zn-O bond lengths are increased (reducing antibonding overlap) which lowers the energy of the red band. At the same time, the interlayer spacing decreases which shortens the out-of-plane Zn-O distances (see Fig. 4), which tends to

View Article Online
DOI: 10.1039/D4NR05206D

increase the anti-bonding overlap and increase the energy of the green band. Eventually, with sufficient in-plane strain, this tendency leads to a transition from a direct bandgap in the layered-ZnO phase to an indirect gap in the hex-ZnO phase. During this transition, the CBM, which is associated with isotropic Zn4*s*-O2*s* antibonding, is stabilised more by the strain-induced increase of in-plane Zn-O separations than the destabilisation from the smaller decrease in interlayer spacing. This CBM stabilization is the main reason for the decrease in E_{gap} in the hex-ZnO phase with increasing biaxial tension.

Starting from a relaxed flat ZnO monolayer, a direct a relatively large positive biaxial strain (8%) has been predicted to be needed to induce a transition from a direct to an indirect gap.[50] Unlike in the presently reported nanofilms, the lack of interlayer interactions in monolayers make the destabilisation of the out-of-plane antibonding states more difficult to achieve. DFT calculations have also been used to study the effect of uniaxial out-of-plane tension on the bulk hex-ZnO phase to induce a phase transformation to the layered phase with a concomitant direct to indirect E_{gap} transition.[51] A related direct to indirect change in E_{gap} has also been reported in DFT studies of the uniaxial compression-induced wz-ZnO → hex-ZnO transition.[48,49] We note that this subtle transition has been confirmed with DFT calculations using hybrid functionals,[51] which confirms that it is not related to the underestimation of E_{gap} magnitudes by GGA functionals.

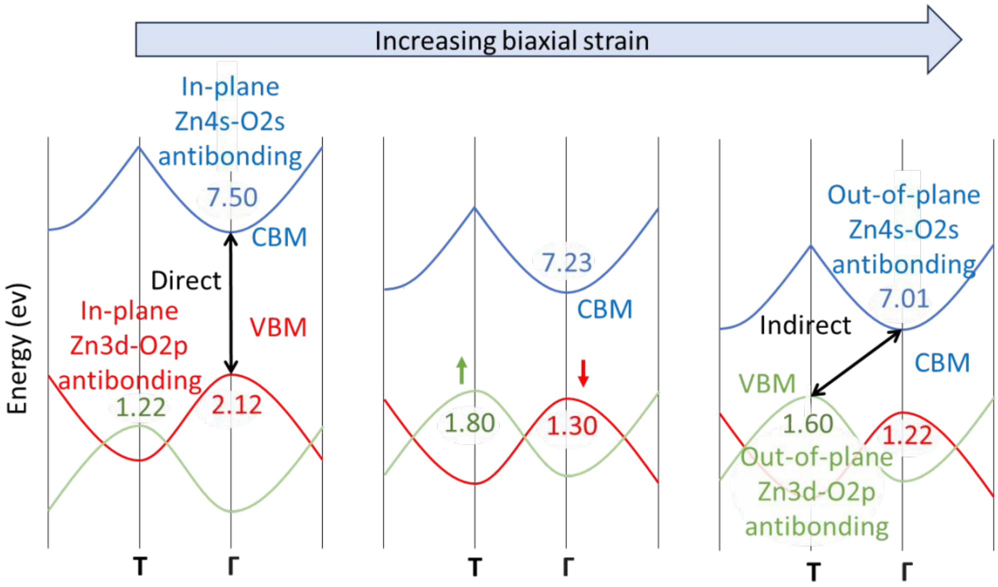

layered-ZnO
(+4% strain)

Phase transformation
+ electronic transition
(+7% strain)

hex-ZnO
(+9% strain)

Figure 6. Calculated band structures during the strain-induced layered-ZnO → hex-ZnO phase transformation of a 5L nanofilm. The three colours correspond to the three labelled dominant

DOI: 10.1039/D4NR05206D

antibonding orbital contributions at **T** (green band) and **Γ** (blue and red bands). The correspondingly coloured numbers indicate the energetic antibonding **k**-COHP contributions at these **k**-points for each band.

In Figure 7 we provide an overview of how the relative energies of the CBM and VBM vary with in-plane biaxial strain with respect to the unstrained case, for all considered nanofilm thicknesses. Nanofilms of all thicknesses exhibit similar general trends with respect their strain-response of CBM and VBM energies, whereby negative strain (*i.e.* in-plane compression) tends to be destabilising, and positive strain (*i.e.* in-plane tension) tends to be stabilising. For the negatively strained regime, where the BCT-ZnO polymorph is favoured, both the VBM and CBM energies increase with increasing in-plane compression for all thicknesses. Here, the VBM is always destabilised more than the CBM (*i.e.* blue bars higher than red bars in Fig. 7) which causes the observed bandgap reduction compared to the corresponding unstrained case (see Fig. 5). In BCT-ZnO the VBM is dominated by contributions from in-plane antibonding orbital overlap, as also found for the layered-ZnO and hex-ZnO polymorphs (see above).

For the positively strained regime in which g-ZnO (i.e. layered-ZnO or hex-ZnO phases) is favoured, for all thicknesses the energy of the CBM (red bars in Fig. 7) gradually decreases with increasing strain. The energy of the VBM, however, is relatively less affected with respect to the that of the corresponding unstrained system for all thicknesses. So, for g-ZnO, the energetic stabilisation of the CBM at **Γ** with increasing biaxial in-plane tension is mainly responsible for the observed strain-induced E_{gap} reduction (see Fig. 5).

View Article Online
DOI: 10.1039/D4NR05206D

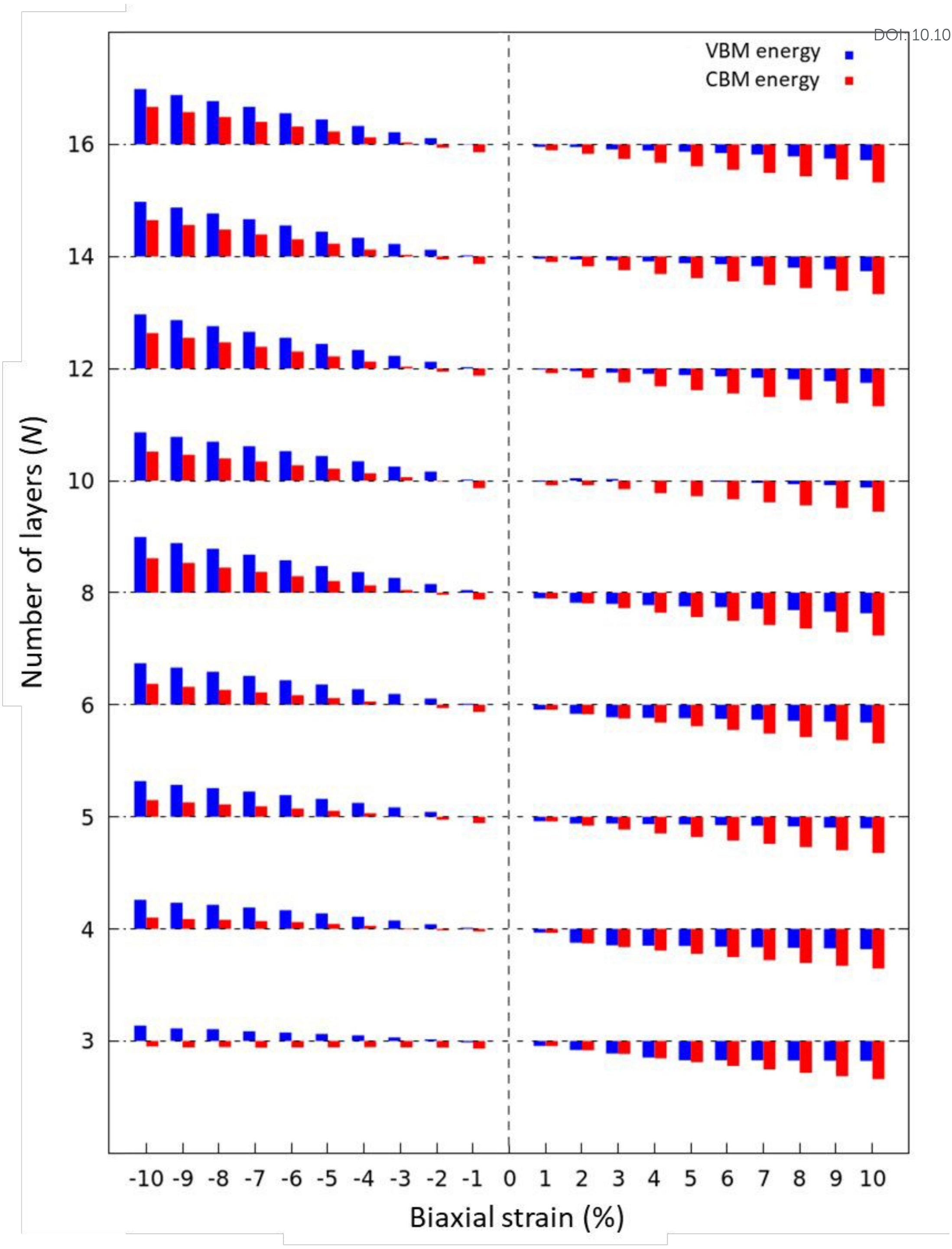

Figure 7. Variation of the energy of the VBM (blue bars) and CBM (red bars) with respect to in-plane biaxial strain for all considered nanofilm thicknesses. The energy variation is taken with respect to the VBM and CBM of the corresponding unstrained nanofilm for each thickness.

Quantum confinement

In addition to the strain-induced changes to E_{gap}, for all curves in Figure 5, we see that nanofilm thickness also affects the magnitude of E_{gap}. Specifically, E_{gap} tends to be largest for the thinnest

View Article Online
DOI: 10.1039/D4NR05206D

nanofilms and becomes progressively smaller with increasing thickness. We note that for the thinnest hex-ZnO films we see a small modulation of this general trend. Here, we find that the E_{gap} magnitudes for the 4L and 6L nanofilms are slightly larger (<0.1 eV) than the corresponding values for the respective 3L and 5L nanofilms. The cause of these small crossovers may be related to the sensitivity of the indirect band gap edges to odd and even numbers of layers for these very thin nanofilms. Generally, the E_{gap} versus thickness relation is also non-linear, where the changes in the magnitude of E_{gap} tend to be largest for thickness changes in the thinnest films and vice versa. This is a clear sign of thickness-dependent quantum confinement (QC). The effect of QC has been previously reported in DFT studies of fully relaxed BCT-ZnO and layered-ZnO nanofilms.[14,47] Generally, the effects of QC are often crucial to take into account when using electronic structure modelling to understand the properties of nanostructured materials for applications (*e.g.* catalysts).[52] To show the effect of QC throughout the strain-induced BCT-ZnO → g-ZnO phase transformation, in Figure 8 we plot the E_{gap} versus nanofilm thickness for: a) the BCT-ZnO nanofilms at 0% strain, and b) the layered-ZnO nanofilms at 4% strain and the hex-ZnO nanofilms for 6% strain. In each case we fit the thickness-dependence of the E_{gap} values with respect to an extrapolated bulk band gap value with an inverse power law (i.e $A \cdot d^{-\alpha}$, where d is the distance between the outer layers of the nanofilm in the *c* direction and A and α are fitted constants). All fits yielded a coefficient of determination (R^2) of greater than 0.99. The magnitude of the coefficient A is inversely related to the effective masses of the carriers in the VBM and CBM (see SI). In idealised particle-in-a-box models these ΔE_{gap} values should be proportional to d^{-2}. In nanosystems that are modelled using DFT, fits of size-dependent ΔE_{gap} values are often better fitted with $\alpha < 2$ due to a more realistic account of the influence of the confining surfaces.[53,54] For unstrained BCT-ZnO we obtain a good fit to the calculated thickness-dependent ΔE_{gap} values with $\alpha = 0.99$, which is comparable with the fit to experimental data on QC in wz-ZnO nanofilms extracted from ref. 55 with $\alpha = 1.05$. The limiting reference E_{gap} value found from the fitting for unstrained BCT-ZnO nanofilms (2.9 eV) lies between the E_{gap} of the optimised bulk BCT-ZnO structure calculated with hybrid DFT calculations (2.26 eV) and many body G_0W_0 calculations (3.41 eV).[56] Note that the reported E_{gap} values for all nanofilms are derived from applying an approximate correction to PBE-calculated values.[18] However, the limiting E_{gap} value from the BCT-ZnO nanofilm fit is 0.33 eV lower than that obtained from a direct application of the correction to the PBE-calculated E_{gap} of bulk BCT-ZnO. This difference could suggest that the bulk-derived correction is less accurate when applied to quantum confined ZnO nanosystems. For the wz-ZnO system we employed the corresponding experimentally determined limiting E_{gap} value of 3.3 eV[55] for our fit. For the hex-ZnO phases we find an α value of 1.35 which is slightly higher than for the BCT-ZnO fit, indicating a correspondingly greater sensitivity to QC. However,

View Article Online
DOI: 10.1039/D4NR05206D

for the layered-ZnO phase the relatively low α value of 0.59 indicates that QC is a much less effective E_{gap} modulator in this type of nanofilm.

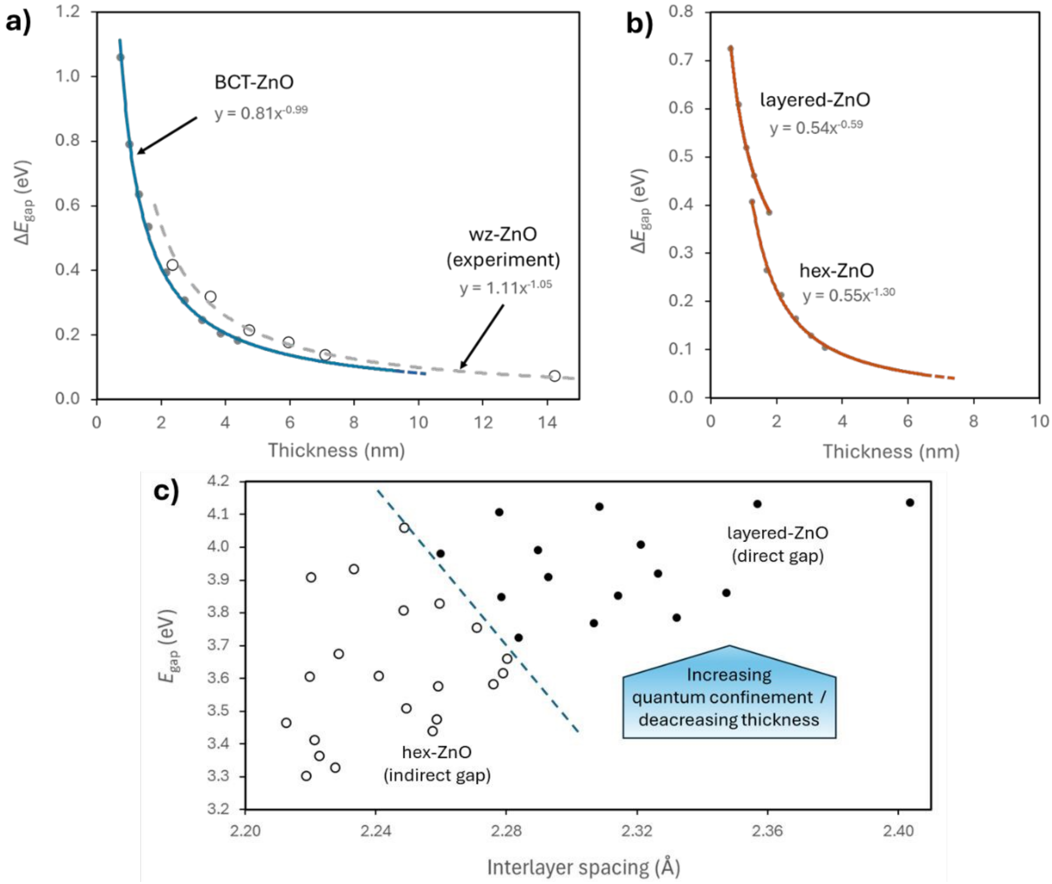

Figure 8. Variance in ΔE_{gap} values with respect to: a) nanofilm thickness for the BCT-ZnO nanofilms at 0% strain (all thicknesses) and experimentally prepared wz-ZnO nanofilms (from ref. 55), b) nanofilm thickness for the layered-ZnO nanofilms at 4% strain (for 3L - 8L) and the hex-ZnO nanofilms for 6% strain (for 6L - 16L), and c) interlayer spacing for the layered-ZnO and hex-ZnO phases for a selected range of strains and thicknesses.

The observed QC effect is found to be due to an increase in the energy of the CBM when the nanofilm thickness decreases. Conversely, the VBM is found to be hardly affected by changes in nanofilm thickness. This contrasting behaviour is in-line with the difference in the effective masses of excited electrons (in the CBM) and holes (in the VBM) in these systems. With a lower effective mass, the respective charge carriers become more mobile (delocalised) and are thus more susceptible to the effects of spatial confinement. Likewise, charge carriers with a higher effective mass are less affected by QC. Generally, wz-ZnO systems are known to have relatively light electrons and heavy holes.[57] We thus expect that thickness-induced QC should have a significantly stronger effect on energy of the CBM than on the energy of the VBM in these nanofilms as confirmed in Fig. 9. We note that a similar effect has been reported in DFT calculations of group III–V semiconductor nanofilms.[58] Nanoporosity is also known to affect the

View Article Online
DOI: 10.1039/D4NR05206D

CBM much more than the VBM in ZnO.[18] For BCT-ZnO the QC-induced E_{gap} variation is contrary to that induced by in-plane strain, which is mainly due to relatively large changes in energy of the VBM. However, for g-ZnO both QC and strain mainly affect the CBM which dominates the observed E_{gap} variations.

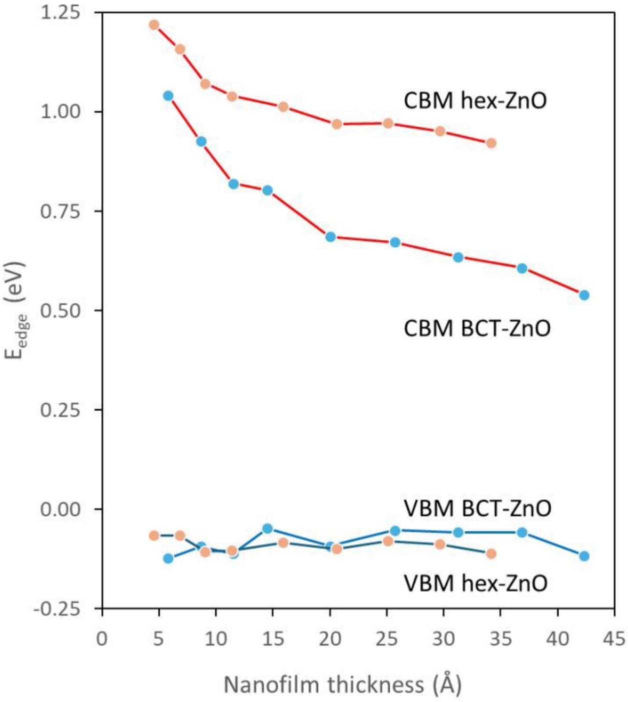

Figure 9. Variance in CBM and VBM energies with respect to nanofilm thickness for BCT-ZnO nanofilms with 0% in-plane biaxial strain and hex-ZnO nanofilms with 6% in-plane biaxial strain.

Combining QC and biaxial strain

To gain more detailed insight into the combined roles of QC and in-plane strain on the electronic structure of our considered nanofilms, we have analysed how the atoms in individual layers contribute to the VBM and CBM. Specifically, we have extracted the **k**-COHP contributions of all atoms in each layer to the VBM and CBM for three nanofilm thicknesses (5L, 10L, and 16L) and for a range of in-plane biaxial strains. In Fig. 10, we compare how the summed atomic **k**-COHP contributions to the VBM for each layer varies for these three nanofilm thicknesses for -10%, 0%, and +3% in-plane biaxial strains. For these combinations of strain and thickness the BCT-ZnO phase is dominant. Clearly, in all cases, the VBM contributions are dominated by Zn and O atoms in the outermost surface layers of the nanofilms with relatively small contributions from atoms from inner layers. With respect to changes in thickness for fixed strains the percentage of the contributions to the VBM from the surface layer atoms is almost constant. As such, the energy

View Article Online
DOI: 10.1039/D4NR05206D

of these localised VBM surface states should not significantly depend on thickness, which is in-line with their relative insensitivity to QC (see Fig. 9).[59,60] For a fixed thickness, increasing in-plane strain from -10% to 0% tends to slightly reduce the VBM contributions in the outermost layers. These outermost surface layer contributions correspond to in-plane antibonding contributions and the reduction in such contributions in consistent with the decrease in the VBM energy for BCT-ZnO films in this strain range (see Fig. 7). Going from 0% to +3% strain some increase in contributions from atoms in sub-surface layers are also seen. These sub-surface contributions are likely linked with the emergence of out-of-plane antibonding contributions to the VBM which we find during the strain-induced layered-ZnO to hex-ZnO transformation (see Fig. 6).

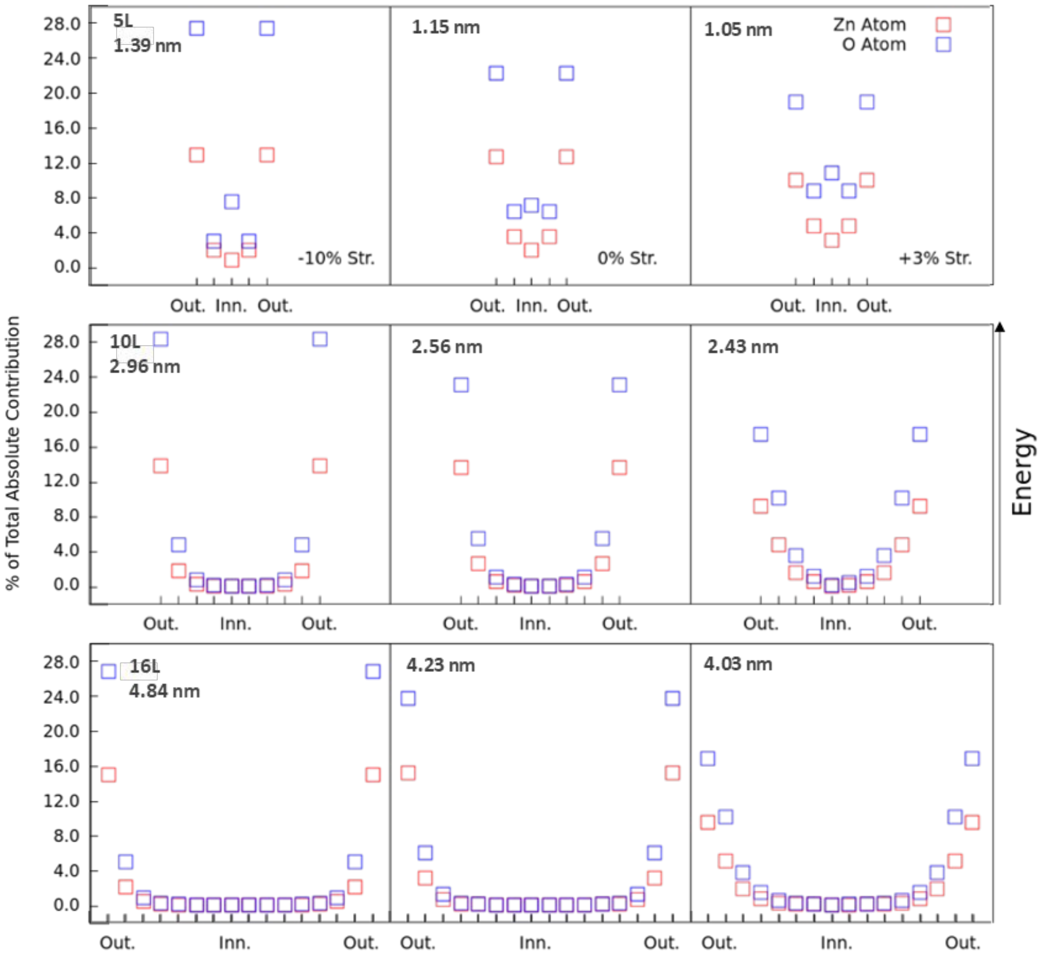

Figure 10. Per-layer summed atomic **k**-COHP contributions to the VBM of 5L, 10L and 16L nanofilms (top to bottom) and -10%, 0% and +3% in-plane biaxial strains (left to right). Contributions are expressed as a percent of the total absolute contribution. The x-axes follow the order of the layers in the out-of-plane *z* direction from one outermost layer (Out.) toward the innermost layer (Inn.) and to the other outermost layer (Out.). In each case the nanofilm thickness in provided in nm.

View Article Online
DOI: 10.1039/D4NR05206D

In Fig. 11, we compare how the summed atomic **k**-COHP contributions to the CBM for each layer varies for the three nanofilm thicknesses for increasing tensile in-plane biaxial strains. For most of these systems the hex-ZnO phase is favoured, apart from the +4% strained 5L nanofilm, for which the layered-ZnO phase is more energetically stable. For this case, the in-plane contributions to the CBM involving unoccupied Zn4*s* and O2*s* orbitals are much larger than the respective out-of-plane contributions. In the absence of significant interlayer interactions all layers are essentially independent and the **k**-COHP analysis in Figure 11 shows that the contribution for each layer is very similar. This situation is gradually changes with increases in thickness and/or biaxial strain but means that the CBM for the layered phase is less susceptible to QC (see Fig. 8). With increased in-plane biaxial tension (to +9% and +14%), the layers in the 5L system are forced to be closer together. This causes a phase transformation to the hex-ZnO polymorph and an increase in out-of-plane anti-bonding Zn4s-O2s contributions to the CBM. Antibonding interactions are less destabilising in situations of reduced orbital overlap and thus their **k**-COHP contributions are dominant for the outer layers of the highly strained 5L system.

Increasing the thickness, for the highest +16% strained 10L and 16L hex-ZnO nanofilms, we find a similar situation to the more strained hex-ZnO 5L systems, where a near surface anti-bonding Zn4s-O2s contributions dominate the CBM. For lower biaxial strains, however, we see the emergence of a similar distinct pattern of **k**-COHP contributions to the CBM for both the 10L and 16L systems. For the +11% strained systems we still see the Zn4*s*-O2*s* antibonding contributions but together with a set of contributions which increase from the outermost layers to the innermost layer. For the +6% strained systems, these latter contributions dominate, and surface contributions are the lowest. The **k**-COHP analysis shows that these contributions come from bonding overlap of unoccupied Zn4*s*-Zn4*s* orbitals (see figure S1 in the ESI). In this pattern of contributions, all layers have a significant contribution, and these contributions have a regular layer-dependency. This implies that the role of each layer and how they interact with each other needs to be considered when interpreting the how the CBM contributions are distributed throughout these nanofilms. From our analysis above (see Figs. 8 and 9), we know that the CBM in hex-ZnO nanofilms is strongly affected by QC, in line with its multi-layer spatially distributed **k**-COHP contributions. The pattern of CBM contributions also implies that QC is felt progressively more strongly going from outer layers to inner layers. This cumulative effect suggests that each layer is incrementally contributing to the overall QC effect. We propose an interpretation of this a situation from the perspective of a monolayer superlattice (*i.e.* a layered system of intercoupled monolayer quantum wells). [59,60]

View Article Online
DOI: 10.1039/D4NR05206D

Monolayer superlattices are typically composed of stacks of single layers of a semiconducting material, which are interleaved with layers of another material to modulate the interactions between the semiconducting monolayers. In our case, the degree of biaxial strain modulates the interactions between ZnO monolayers in the g-ZnO system. Taking the +6% 10L case as an example, the CBM corresponds to a wavefunction (WF) that is dominated by interlayer bonding interactions. Treating each ZnO monolayer as a quantum well leads to a discretisation of the effect of QC on this WF. Starting from outside the system, where the WF has its minimum value, it will increase when entering the first monolayer well. When moving to the next monolayer the interlayer coupling will determine the degree of WF decay, and thus the

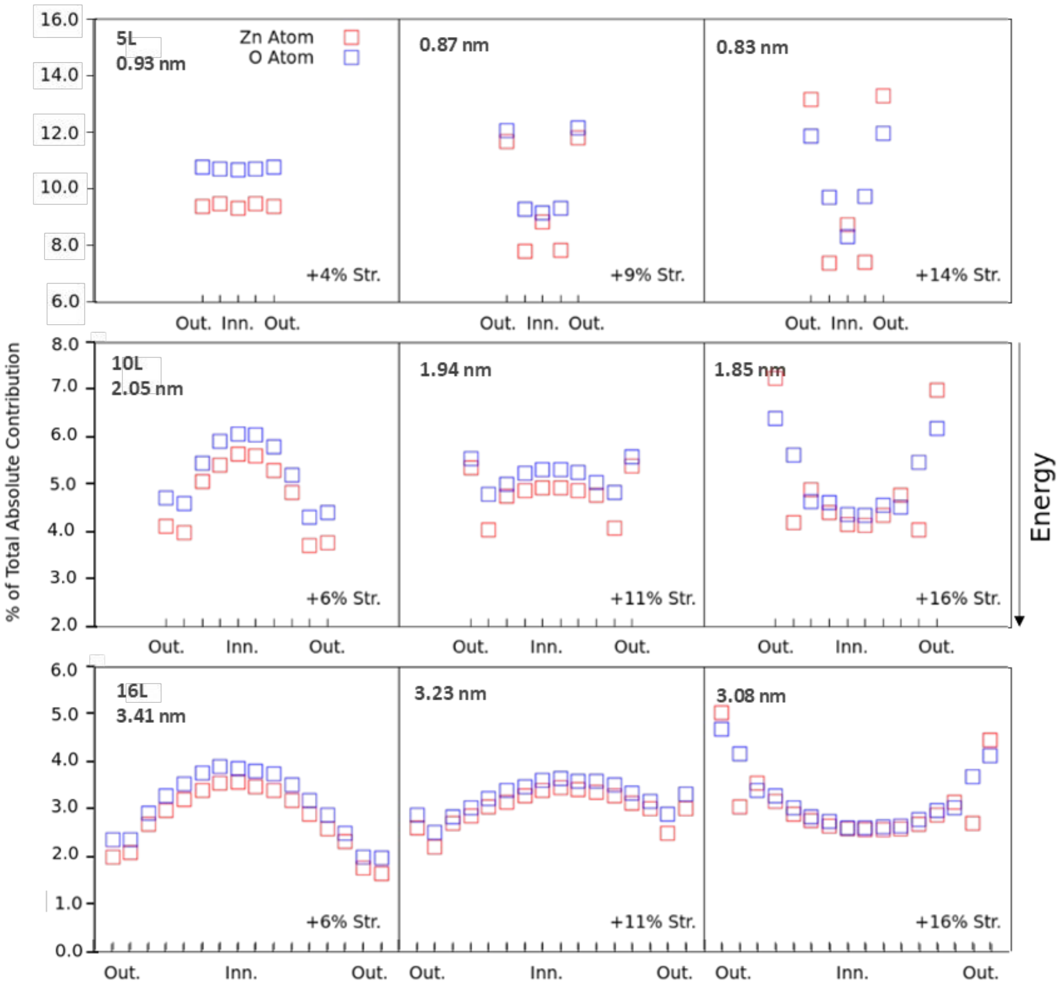

Figure 11. Per-layer summed atomic **k**-COHP contributions to the CBM of nanofilms with 5L for +4%, +9% and +14% in-plane biaxial strains and for 10L and 16L thicknesses and +6%, +11% and +16% in-plane biaxial strains. The contributions per-layer are expressed as a percent of the total absolute contribution. The x-axes follow the order of the layers in the out-of-plane *z* direction from one outermost layer (Out.) toward the innermost layer (Inn.) and to the other outermost layer (Out.). In each case the nanofilm thickness in provided in nm.

View Article Online
DOI: 10.1039/D4NR05206D

magnitude of the WF in the next ZnO layer. When the decay is less than 100%, the WF magnitude will increase in a step-wise layer-by-layer manner until the centre and then, by symmetry, will decay again in the same manner to the farthest edge of the nanofilm. In this way, QC acts on the fully nanofilm system but is modulated depending on the interlayer coupling. Such a discretised WF for monolayer superlattice is schematically shown in Fig. 12a. These results show that hex-ZnO can be thought of as a lateral monolayer superlattice in which in-plane biaxial strain can significantly modulate the interlayer coupling. Upon increased biaxial strain there is a gradual transition from Zn4*s*-Zn4*s* interlayer bonding overlap to anti-bonding Zn4*s*-O2*s* overlap. Upon the corresponding interior-to-surface shift in the character of the WF, transmission of QC to the system is diminished (Fig. 12b,c). This shows that the electronic response of g-ZnO nanofilms can be sensitively tuned by strain and thickness. In particular, the ability to shift between surface states and QC-susceptible states could open up new application potential (e.g. sensing, catalysis, optoelectronics).

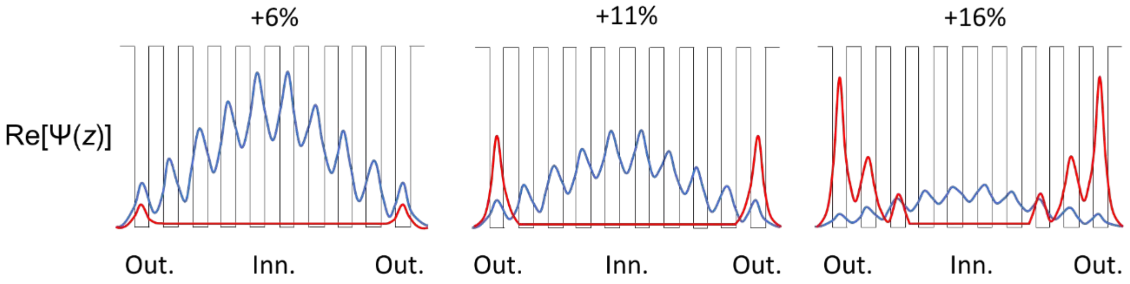

Figure 12. Schematic representation of the approximate magnitude of the Zn4s- Zn4s bonding (blue) and Zn4s-O2s antibonding (red) contributions to a monolayer superlattice WF associated with the CBM for the 10L hex-ZnO system for +6%, +11% and +16% in-plane biaxial strain (see also Fig. 11). The x-axes follow the order of the layers in the out-of-plane *z* direction from one outermost layer (Out.) toward the innermost layer (Inn.) and to the other outermost layer (Out.).

Conclusions

We provide a detailed investigation of the structural and electronic properties of ZnO nanofilms with thicknesses from 3L to 16L, for a wide range of compressive and tensile biaxial strains. This parameter regime allows us to follow the experimentally confirmed strain-induced BCT-ZnO ↔ g-ZnO polymorphic phase transition. Our study is distinguished by its widespread application of COHP-based analysis. Such an approach allows for an orbital level system characterisation and, as far as we are aware, has not previously been applied to analyse nanoscale phase transformations. For all considered film thicknesses and compressive strains the BCT-ZnO phase is the most stable. With tensile biaxial strain the barrierless structural transformation to the g-

View Article Online
DOI: 10.1039/D4NR05206D

ZnO polymorphic phase is favoured. Generally, with sufficient positive or negative biaxial strain, the E_{gap} is reduced. Likewise, the increase in nanofilm thickness also leads to a E_{gap} decrease. Our COHP-based analysis reveals several detailed insights into these structural and electronic tendencies. Generally, our results highlight the intimate relation between structure, bonding and electronic properties. We highlight, for example, that all three of these properties serve to distinguish the quasi-2D layered-ZnO phase from the 3D hex-ZnO phase, both often collectively referred to as the g-ZnO phase. For strains favouring the g-ZnO phase, variations in the CBM drive the strain-related change in E_{gap}. However, for the BCT-ZnO dominated strain/thickness regime, the VBM mainly determines the strain-dependent changes in E_{gap}. With respect to increases in thickness, for both BCT-ZnO and g-ZnO, the E_{gap} reduction is due to QC acting on the CBM. We use layer-by-layer k-COHP-based analysis to reveal the detailed nature of the CBM and VBM, thus elucidating their respective susceptibility to QC. This analysis shows that the CBM in g-ZnO nanosystems can be sensitively tuned by strain and/or thickness between being dominated by QC-resistant localised surface contributions or having a QC-dependent spatially-distributed character. The competition between these two states can be rationalised from a monolayer superlattice perspective. Here, the superlattice electronic state can be tuned by the degree of strain/thickness-dependent interlayer interactions and their bonding or antibonding character, rather than by fixed intervening barrier layers. This dramatic electronic tunability could pave the way to a range of new applications (e.g. photocatalysis, optoelectronics, sensors).

Author contributions

STB formulated the original research concept and directed the project. RMS and ID performed the DFT calculations. RMS performed the COHP calculations. STB and RMS prepared the original draft of the paper. All authors contributed to the analysis and interpretation of the results and revising of the final draft.

Conflicts of interest

There are no conflicts to declare.

Data availability

Data for this article, including VASP OUTCAR files and optimised atomic coordinates for all nanofilms considered are available at the NOMAD repository at https://doi.org/10.17172/NOMAD/2024.12.06-3.

DOI: 10.1039/D4NR05206D

Acknowledgements

Support is acknowledged from the MICINN-funded PID2021-127957NB-I00, PID2021-126076NB-I00, TED2021-129506B-C22, and TED2021-132550B-C21 project grants, and the Maria de Maeztu program for Spanish Structures of Excellence (CEX2021-001202-M) and project grants 2021SGR00354 and 2021SGR00079 funded by the Generalitat de Catalunya. F.V. thanks the ICREA Academia Award 2023 Ref. Ac2216561. I.D. acknowledges support from the Eskisehir Technical University (ESTÜ-BAP-21GAP085).

References

---

1. A. Navrotsky, Energetic clues to pathways to biomineralization: Precursors, clusters, and nanoparticles, *Proc. Nat. Acad. Sci.,* 2004, **101**, 12096.

2. S. Yang , F. Liu , C. Wu and S. Yang, Tuning surface properties of low dimensional materials via strain engineering, *Small*, 2016, **12**, 4028–4047.

3. Q. Yun *et al.*, Recent Progress on Phase Engineering of Nanomaterials, *Chem. Rev.,* 2023, **123**, 13489−13692.

4. Z. L. Wang, Nanostructures of zinc oxide, *Mater. Today*, 2004, **7**, 26-33.

5. S. Rahaa and M. Ahmaruzzaman, ZnO nanostructured materials and their potential applications: progress, challenges and perspectives, *Nanoscale Adv.*, 2022, **4**, 1868-1925

6. C. Tusche, H. L. Mayerheim and J. Kirschner, Observation of Depolarized ZnO(0001) Monolayers: Formation of Unreconstructed Planar Sheets, *Phys. Rev. Lett.,* 2007, **99**, 026102.

7. P. Zhao, X. Guan, H. Zheng, S. Jia, L. Li, H. Liu, L. Zhao, H. Sheng, W. Meng, Y. Zhuang, J. Wu, L. Li and J. Wang, Surface- and Strain-Mediated Reversible Phase Transformation in Quantum-Confined ZnO Nanowires, *Phys. Rev. Lett.,* 2019, **123**, 216101.

8. C. L. Freeman, F. Claeyssens, N. L. Allan and J. H. Harding, Graphitic nanofilms as precursors to wurtzite films: theory, *Phys. Rev. Lett.,* 2006, **96**, 066102.

9. A. J. Kulkarni, M. Zhou, K. Sarasamak and S. Limpijumnong, Novel Phase Transformation in ZnO Nanowires under Tensile Loading, *Phys. Rev. Lett.,* 2006, **97**, 105502.

10. L. Zhang and H. Huang, Structural transformation of ZnO nanostructures, *Appl. Phys. Lett.*, 2007, **90**, 023115.

11. B. J. Morgan, Preferential stability of the d-BCT phase in ZnO thin films, *Phys. Rev. B: Condens. Matter Mater. Phys.*, 2009, **80**, 174105.

12. I. Demiroglu and S. T. Bromley, Nanofilm versus Bulk Polymorphism in Wurtzite Materials, *Phys. Rev. Lett.*, 2013, **110**, 245501.

13. F. Viñes, O. Lamiel-Garcia, F. Illas and S.T. Bromley, Size dependent structural and polymorphic transitions in ZnO: from nanocluster to bulk, *Nanoscale,* 2017*,* **9**, 10067–10074.

14. S. Conejeros, N. L. Allan, F. Claeyssens and J. N. Hart, Graphene and novel graphitic ZnO and ZnS nanofilms: the energy landscape, nonstoichiometry and water dissociation, *Nanoscale Adv.*, 2019, **1**, 1924.

View Article Online
DOI: 10.1039/D4NR05206D

15. J. Carrasco, F. Illas and S. T. Bromley, Ultralow-Density Nanocage-Based Metal-Oxide Polymorphs, *Phys. Rev. Lett.* 2007, **99**, 235502.

16. M. A. Zwijnenburg, F. Illas and S. T. Bromley, Apparent Scarcity of Low-Density Polymorphs of Inorganic Solids, *Phys. Rev. Lett.,* **104**, 175503.

17. M. A. Zwijnenburg and S. T. Bromley, Structure direction in zinc oxide and related materials by cation substitution: an analogy with zeolites, *J. Mater. Chem.*, 2011, **21**, 15255.

18. I. Demiroglu, S. Tosoni, F. Illas and S. T. Bromley, Bandgap engineering through nanoporosity, *Nanoscale*, 2014, **6**, 1181-1187.

19. L. Lin, Z. Zeng, Q. Fu and X. Bao, Strain and support effects on phase transition and surface reactivity of ultrathin ZnO films: DFT insights, *AIP Advances,* 2020, **10**, 125125.

20. L. Lin, Z. Zeng, Q. Fu and X. Bao, Achieving flexible large-scale reactivity tuning by controlling the phase, thickness and support of two-dimensional ZnO, *Chem. Sci.*, 2021, **12**, 15284.

21. Y. Zhao, N. Liu, S. Zhou and J. Zhao, Two-dimensional ZnO for the selective photoreduction of CO_2, *J. Mater. Chem. A*, 2019, **7**, 16294–16303.

22. B. Meyer and D. Marx, Density-functional study of the structure and stability of ZnO surfaces, *Phys. Rev. B*, 2003, **67**, 035403.

23. G. Kresse, O. Dulub and U. Diebold, Competing stabilization mechanism for the polar ZnO (0001)-Zn surface, *Phys. Rev. B*, 2003, **68**, 245409.

24. D. Mora-Fonz, T. Lazauskas, M. R. Farrow, C. R. A. Catlow, S. M. Woodley and A. A. Sokol, Why are polar surfaces of ZnO stable?, *Chem. Mater.*, 2017, **29**, 5306.

25. L-Z. Xu, Y-L. Liu, H.-B. Zhou, L.-H. Liu, Y. Zhang and Guang-Hong Lu, Ideal strengths, structure transitions, and bonding properties of a ZnO single crystal under tension, *J. Phys.: Condens. Matter*, 2009, **21**, 495402.

26. W. Sangthong, J. Limtrakul, F. Illas and S. T. Bromley, Predicting transition pressures for obtaining nanoporous semiconductor polymorphs: oxides and chalcogenides of Zn, Cd and Mg, *Phys. Chem. Chem. Phys.*, 2010, **12**, 8513-8520.

27. D. Zagorac, J. C. Schön, J. Zagorac and M. Jansen, Prediction of structure candidates for zinc oxide as a function of pressure and investigation of their electronic properties, *Phys. Rev. B*, 2014, **89**, 075201.

28. B. Wei, K. Zheng, Y. Ji, Y. Zhang, Z. Zhang and X. Han, Size-Dependent Bandgap Modulation of ZnO Nanowires by Tensile Strain, *Nano Lett.*, 2012, **12**, 4595–4599.

29. J. Wang, A. J. Kulkarni, K. Sarasamak, S. Limpijumnong, F. J. Ke and M. Zhou, Molecular dynamics and density functional studies of a body-centered-tetragonal polymorph of ZnO, *Phys. Rev. B*, 2007, **76**, 172103.

30. J. Zhang, Phase transformation and its effect on the piezopotential in a bent zinc oxide nanowire, *Nanotechnology*, 2021, **32**, 075404.

31. M-R. He, R. Yu and J. Zhu, Reversible Wurtzite–Tetragonal Reconstruction in ZnO(10-10) Surfaces, *Angew. Chem. Int. Ed.*, 2012, **51**, 7744 –7747.

32. B. Morgan, First-principles study of epitaxial strain as a method of B4→BCT stabilization in ZnO, ZnS, and CdS, *Phys. Rev. B*, 2010, **82**, 153408.

33. D. Wu, M. G. Lagally and F. Liu, Stabilizing Graphitic thin films of wurtzite materials by epitaxial strain, *Phys. Rev. Lett.*, 2011, **107**, 236101.

View Article Online
DOI: 10.1039/D4NR05206D

34. J. P. Perdew, K. Burke and M. Ernzerhof, Generalized Gradient Approximation Made Simple, *Phys. Rev. Lett.*, 1996, **77**, 3865.

35. G. Kresse, J. Furthmüller, Efficiency of Ab-Initio Total Energy Calculations for Metals and Semiconductors Using a Plane-Wave Basis Set, *Computational Materials Science*, 1996, **6**, 15–50.

36. G. Kresse and J. Furthmüller, Efficient Iterative Schemes for Ab Initio Total-Energy Calculations Using a Plane-Wave Basis Set, *Phys. Rev. B: Condens. Matter Mater. Phys.*, 1996, **54**, 11169 —11186.

37. M. Kalaya, H. H. Karta, S. Ö. Karta and T. Çağın, Elastic properties and pressure induced transitions of ZnO polymorphs from first-principle calculations, *J. Alloys Compd.*, 2009, **484**, 431–438.

38. J. E. Jaffe, J. A. Snyder, Z. Lin and A. C. Hess, LDA and GGA calculations for high-pressure phase transitions in ZnO and MgO, *Phys. Rev. B*, 2000, **62**, 1660.

39. M. P. Molepo and D. P. Joubert, Computational study of the structural phases of ZnO, *Phys. Rev. B*, 2011, **84**, 094110.

40. P.E. Blöch, Projector Augmented-Wave method, *Phys. Rev. B,* 1994, **50**, 17953.

41. H. J. Monkhorst and J. D. Pack, Special Points for Brillouin-Zone Integrations. *Phys. Rev. B*, 1976, **13**, 5188.

42. R. Dronskowski, P. E. Blöchl, Crystal Orbital Hamilton Populations (COHP). Energy-Resolved Visualization of Chemical Bonding in Solids based on Density-Functional Calculations. *J. Phys. Chem.* 1993, **97**, 8617—8624

43. S. Maintz, V. L. Deringer, A. L. Tchougreeff, R. Dronskowski Analytic Projection from Plane-Wave and PAW Wavefunctions and Application to Chemical-Bonding Analysis in Solids. *J. Comput. Chem.* 2013, **34**, 2557—2567.

44. S. Maintz, V. L. Deringer, A. L. Tchougreeff, R. Dronskowski LOBSTER: A tool to extract chemical bonding from plane-wave based DFT. *J. Comput. Chem.* 2016, **37**, 1030—1035.

45. X. Peng, Q. Wei, A. Copple, Strain-Engineered Direct-Indirect Band Gap Transition and Its Mechanism in Two-Dimensional Phosphorene, *Phys. Rev. B*, 2014, **90**, 085402.

46. S. M. Kozlov, I. Demiroglu, K. M. Neyman and S. T. Bromley, Reduced ceria nanofilms from structure prediction, *Nanoscale*, 2015, **7**, 4361.

47. L. Sponza, J. Goniakowski and C. Noguera, Confinement effects in ultrathin ZnO polymorph films: Electronic and optical properties, *Phys. Rev. B*, 2016, **93**, 195435.

48. Y. Wanga, W. Tang, J. Zhu and J. Liu, Strain induced change of band structure and electron effective mass in wurtzite ZnO: A first-principles study, *Comp. Mater. Sci.*, 2015, 145–149.

49. Y. Zhang, Y-H. Wen, J-C. Zheng and Z-Z. Zhuc, Direct to indirect band gap transition in ultrathin ZnO nanowires under uniaxial compression, *Appl. Phys. Lett.*, 2009, **94**, 113114.

50. R. Das, B. Rakshit, S. Debnath and P. Mahadevan, Microscopic model for the strain-driven direct to indirect band-gap transition in monolayer MoS_2 and ZnO, *Phys. Rev. B*, 2014, **89**, 115201.

51. B. Rakshit and P. Mahadevan, Indirect to direct bandgap transition under uniaxial strain in layered ZnO, *Appl. Phys. Lett.*, 2013, **102**, 143116.

52. E. Inico, C. Saetta, G. Di Liberto, Impact of quantum size effects to the band gap of catalytic materials: a computational perspective, *J. Phys.: Condens. Matter* 2024, **36**, 361501.

View Article Online
DOI: 10.1039/D4NR05206D

53. N. S. Mohammad, Understanding quantum confinement in nanowires: basics, applications and possible laws, *J. Phys.: Condens. Matter*, 2014, **26**, 423202.

54. P. Zhang, Z. Liu, W. Duan, F. Liu and J. Wu, Topological and electronic transitions in a Sb(111) nanofilm: The interplay between quantum confinement and surface effect, *Phys. Rev. B*, 2012, **85**, 201410(R).

55. A. Barnasas, N. Kanistras, A. Ntagkas, D.I. Anyfantis, A. Stamatelatos, V. Kapaklis, N. Bouropoulos, E. Mystiridou, P. Poulopoulos, C. S. Garoufalis and S. Baskoutas, Quantum confinement effects of thin ZnO films by experiment and theory, *Phys. E*, 2020, **120**, 114072.

56. L. Sponza, J. Goniakowski and C. Noguera, Structural, electronic, and spectral properties of six ZnO bulk polymorphs, *Phys. Rev. B*, 2015, **91**, 075126.

57. H. Morkoç, Ü. Özgür, Zinc Oxide: Fundamentals, Materials and Device Technology. Germany, Wiley, 2008.

58. L. A. Cipriano, G. Di Liberto, S. Tosoni and G. Pacchioni , Quantum confinement in group III–V semiconductor 2D nanostructures, *Nanoscale*, 2020, **12**, 17494.

59. S. Y. Ren, Two types of electronic states in one-dimensional crystals of finite length, *Ann. Physics*, 2002, **301**, 22–30.
60. P. Pereyra, The transfer matrix method and the theory of finite periodic systems. From heterostructures to superlattices, *pss b*, 2022, **259**, 2100405.

Data availability statement for:

View Article Online
DOI: 10.1039/D4NR05206D

Tuning the Electronic Properties of ZnO Nanofilms via Strain-induced Structural Phase Transformations and Quantum Confinement

Raul Morales-Salvador, Ilker Demiroglu, Francesc Viñes, Stefan T. Bromley*

* Corresponding author: s.bromley@ub.edu

Data for this article, including VASP output files and corresponding optimised atom coordinates for all nanofilm structures, are available at the NOMAD repository at https://doi.org/10.17172/NOMAD/2024.12.06-3.